CWP-589

Interval anisotropic parameter estimation using velocity-independent layer stripping

Xiaoxiang Wang & Ilya Tsvankin
Center for Wave Phenomena, Geophysics Department, Colorado School of Mines, Golden, Colorado 80401

ABSTRACT
Moveout analysis of long-spread P-wave data is widely used to estimate the key time-processing parameter η in layered VTI media. Inversion for interval η values, however, suffers from instability caused by the tradeoff between the effective moveout parameters and by the subsequent error amplification during Dix-type layer stripping. Here, we propose an alternative approach to interval parameter estimation based on the velocity-independent layer-stripping method of Dewangan & Tsvankin (2006). This method makes it possible to compute the interval moveout in a layer of interest without knowledge of the medium parameters in the overburden. Then the interval traveltimes are inverted for the normal-moveout velocity ($V_{\rm nmo}$) and η using the single-layer nonhyperbolic moveout equation. Thus, the layer stripping of η in the conventional method is replaced by the much more stable stripping of reflection traveltimes. We also develop the 3D version of the layer-stripping method and apply it to interval parameter estimation for orthorhombic media using wide-azimuth P-wave data. The superior accuracy and stability of our algorithm is illustrated on ray-traced synthetic data for typical layered VTI and orthorhombic models. Even small correlated noise in reflection traveltimes produces substantial distortions in the effective η, and for some models, even in the effective $V_{\rm nmo}$. As a result, the inter val η values estimated by the conventional Dix-type method may be highly inaccurate. In contrast, the output of our layer-stripping algorithm proves to be insensitive to mild correlated traveltime errors. The algorithm is also tested on wide-azimuth P-wave reflection data recorded above a fractured reservoir at Rulison field in Colorado. The interval moveout parameters estimated by the velocity-independent layer stripping in the shale layer above the reservoir are more plausible and stable than those obtained by the Dix-type method.

Key words: Anisotropy, interval parameters, layer stripping, nonhyperbolic moveout, wide-azimuth data, layer-cake models

1 INTRODUCTION

Traveltime analysis of surface reflection data yields effective moveout parameters for the whole section above the reflector. However, for purposes of migration velocity analysis, AVO (amplitude-variation-with-offset) inversion, and seismic fracture characterization, it is necessary to estimate interval parameters, which is done using layer-stripping (e.g., Dix, 1955; Grechka & Tsvankin, 1998; Grechka *et al.*, 1999) or tomographic (e.g., Stork, 1992; Grechka *et al.*, 2002) methods.

The conventional Dix (1955) equation, derived for horizontally layered isotropic media, helps to obtain the interval NMO (normal-moveout) velocity using the NMO velocities for the reflections from the top and bottom of a layer. The Dix equation remains valid for NMO velocities of all pure (non-converted) modes in layer-cake VTI (transversely isotropic with a vertical symmetry axis) media. For 3D wide-azimuth data from layered azimuthally anisotropic media, the effective NMO velocity can be obtained by Dix-type averaging of the interval NMO ellipses (Grechka *et al.*, 1999). Then, as

long as the model is laterally homogeneous, the interval NMO velocity or ellipse can be found using Dix-type layer stripping.

NMO velocity and conventional-spread reflection moveout, however, are often insufficient to build the velocity field for anisotropic media, even in the time domain. This explains the importance of using nonhyperbolic (long-spread) reflection moveout in anisotropic parameter estimation. In VTI media, all P-wave time-domain signatures depend on just two parameters, the NMO velocity from a horizontal reflector ($V_{\rm nmo}$) and the anellipticity coefficient η (Alkhalifah & Tsvankin, 1995; Tsvankin, 2005). While $V_{\rm nmo}$ controls the conventional-spread reflection moveout of horizontal P-wave events, η is responsible for the deviation from hyperbolic moveout at long offsets. Most implementations of nonhyperbolic moveout inversion for VTI media (e.g., Alkhalifah, 1997; Toldi *et al.*, 1999; Grechka & Tsvankin, 1998) are based on the moveout equation of Alkhalifah & Tsvankin (1995) which represents an adaptation of the more general Tsvankin–Thomsen (1994) equation for P-waves.

An alternative algorithm for η estimation operates with the dip dependence of P-wave NMO velocity (Alkhalifah & Tsvankin, 1995). Although the dip-moveout inversion is relatively stable, it requires the presence of dipping reflectors under the formation of interest.

The parameters $V_{\rm nmo}$ and η are usually estimated from a 2D semblance scan on long-spread data (the maximum offset should reach two reflector depths) from a horizontal reflector. Despite its relative simplicity, nonhyperbolic moveout inversion suffers from the instability caused by the tradeoff between $V_{\rm nmo}$ and η on any finite spread. Grechka & Tsvankin (1998) found that even small traveltime errors, which could be considered as insignificant in data processing, may cause large errors in the estimated η. For layered VTI media, the error is amplified in the layer-stripping process, which may cause unacceptable distortions in the interval η values.

The Alkhalifah–Tsvankin (1995) equation was extended to azimuthally anisotropic models by employing the azimuthally dependent NMO velocity (i.e., the NMO ellipse) and parameter η (Grechka & Tsvankin, 1999; Xu & Tsvankin, 2006). Here, we consider azimuthally anisotropic media with orthorhombic symmetry typical for fractured reservoirs (Schoenberg & Helbig, 1997; Bakulin *et al.*, 2000; Grechka & Kachanov, 2006). Nonhyperbolic moveout of P-waves in an orthorhombic layer with a horizontal symmetry plane is governed by the azimuths of the vertical symmetry planes, the symmetry-plane NMO velocities ($V_{\rm nmo}^{(1)}$ and $V_{\rm nmo}^{(2)}$) responsible for the NMO ellipse, and three anellipticity coefficients $\eta^{(1,2,3)}$ (Grechka & Tsvankin, 1999). For layered orthorhombic media, P-wave moveout is described by the Alkhalifah–Tsvankin equation with the effective moveout parameters (Xu & Tsvankin, 2006; Vasconcelos & Tsvankin, 2006). Since the symmetry-plane NMO velocities and parameters $\eta^{(1,2,3)}$ depend on the fracture compliances and orientations (Bakulin *et al.*, 2000), nonhyperbolic moveout inversion can help in building physical models for reservoir characterization. Also, the parameters $V_{\rm nmo}^{(1,2)}$ and $\eta^{(1,2,3)}$ are sufficient to perform all time-processing steps in orthorhombic models, such as NMO and DMO (dip moveout) correction, and prestack and poststack time migration (Grechka & Tsvankin, 1999). Still, estimation of the interval parameters $\eta^{(1,2,3)}$ for layered orthorhombic media still suffers from the instability caused by the tradeoff between the effective parameters $V_{\rm nmo}$ and η and by the error amplification in the layer stripping.

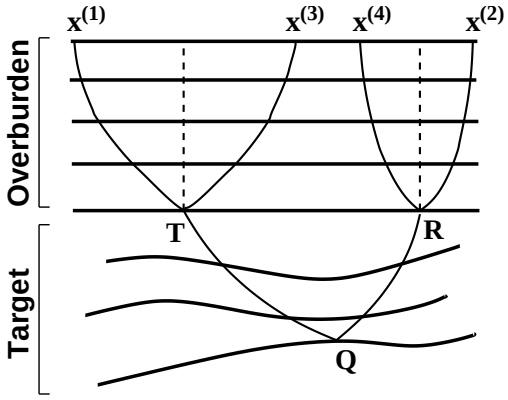

Figure 1. 2D diagram of the layer-stripping algorithm for pure-mode reflections (after Dewangan & Tsvankin, 2006). Points T and R are located at the bottom of the laterally homogeneous overburden. The leg $x^{(1)}$T is shared by the target reflection $x^{(1)}$TQR$x^{(2)}$ and the overburden event $x^{(1)}$T$x^{(3)}$; the leg R$x^{(2)}$ is shared by the reflections $x^{(1)}$TQR$x^{(2)}$ and $x^{(2)}$R$x^{(4)}$.

Here, we propose an alternative approach to interval moveout parameter estimation based on the velocity-independent layer-stripping method of Dewangan & Tsvankin (2006). This layer-stripping algorithm, which operates with reflection traveltimes, produces accurate interval long-spread reflection moveout, which can then be inverted for the interval parameters. We discuss both the 2D version of the method designed for layered VTI media and the 3D implementation for wide-azimuth data from layered orthorhombic media. Using ray-traced synthetic data for typical layered anisotropic media, we demonstrate that in contrast to Dix-type inversion, our method remains robust in the presence of typical correlated noise in reflection traveltimes. Finally, we apply the layer-stripping algorithm to wide-azimuth P-wave data acquired over a fractured reservoir at Rulison field in Colorado.

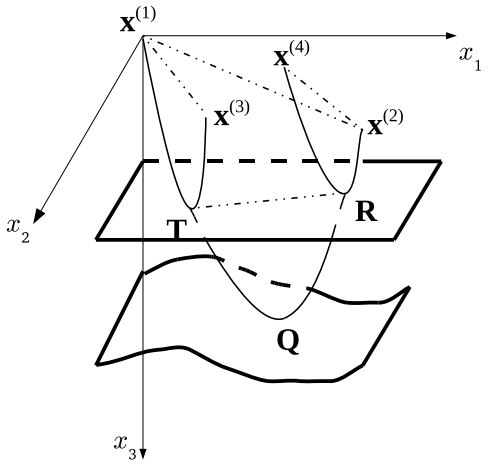

Figure 2. 3D diagram of the layer-stripping algorithm. Points **T** and **R** are located at the bottom of the laterally homogeneous overburden. The sources and receivers ($\mathbf{x}^{(1)}$, $\mathbf{x}^{(2)}$, $\mathbf{x}^{(3)}$ and $\mathbf{x}^{(4)}$) are located at the surface but not necessarily along a straight line. The reflection point **Q** is at the bottom (possibly curved) of the target layer. The leg $\mathbf{x}^{(1)}\mathbf{T}$ is shared by the reflections $\mathbf{x}^{(1)}\mathbf{TQR}\mathbf{x}^{(2)}$ and $\mathbf{x}^{(1)}\mathbf{T}\mathbf{x}^{(3)}$; the leg $\mathbf{R}\mathbf{x}^{(2)}$ is shared by the reflections $\mathbf{x}^{(1)}\mathbf{TQR}\mathbf{x}^{(2)}$ and $\mathbf{x}^{(2)}\mathbf{R}\mathbf{x}^{(4)}$.

2 VELOCITY-INDEPENDENT LAYER STRIPPING

The velocity-independent layer-stripping algorithm introduced by Dewangan & Tsvankin (2006) is based on the PP + PS = SS method of Grechka & Tsvankin (2002). This algorithm is entirely data-driven and, if the model assumptions are satisfied, does not require knowledge of the velocity field anywhere in the medium.

2.1 Layer stripping in 2D

Figure 1 shows 2D ray trajectories of pure-mode (non-converted) reflections from the top and bottom of the target zone. The incidence plane is supposed to represent a symmetry plane for the model as a whole so that wave propagation is two-dimensional. The target zone can be heterogeneous and can include interval curved interfaces. Each layer in the overburden has to be laterally homogeneous with a horizontal symmetry plane, so that the raypath of any reflection from the top of the target zone is symmetric with respect to the reflection point (e.g., points T or R in Figure 1). By equalizing time slopes on common-receiver gathers, we can identify the overburden reflection $x^{(1)}\mathrm{T}x^{(3)}$ that shares the downgoing leg $x^{(1)}\mathrm{T}$ with the target event $x^{(1)}\mathrm{TQR}x^{(2)}$ (Dewangan & Tsvankin, 2006). Likewise, we can find the overburden reflection $x^{(2)}\mathrm{R}x^{(4)}$ that has the same upgoing leg $\mathrm{R}x^{(2)}$ as the target event $x^{(1)}\mathrm{TQR}x^{(2)}$. Then, the interval reflection traveltime t^{int} in the target zone can be computed as

$$t^{\mathrm{int}}(T,R) = t^{\mathrm{eff}}(x^{(1)},x^{(2)}) - \frac{1}{2}\left[t^{\mathrm{ovr}}(x^{(1)},x^{(3)}) + t^{\mathrm{ovr}}(x^{(2)},x^{(4)})\right]. \quad (1)$$

Here, the superscripts *eff* and *ovr* refer to the reflection traveltimes from the target reflector and the bottom of the overburden, respectively. The corresponding source-receiver pair (T,R) has the following horizontal coordinates:

$$x_{_T} = \frac{x^{(1)}+x^{(3)}}{2}, \qquad x_{_R} = \frac{x^{(2)}+x^{(4)}}{2}. \quad (2)$$

Equation 1 and 2 yield the interval reflection moveout function in the target zone without any information about the velocity model.

2.2 Layer stripping in 3D

The 3D version of the layer-stripping algorithm does not impose any restriction on the target zone, but each layer in the overburden still has to be laterally homogeneous with a horizontal symmetry plane. For wide-azimuth data (Figure 2), identifying the target and overburden reflections with the same ray segments requires estimating two orthogonal horizontal slowness components from time slopes on wide-azimuth data. In Figure 2, the horizontal slownesses of the target (eff) and overburden (ovr) reflections at location $\mathbf{x}^{(1)} = [x_1^{(1)}, x_2^{(1)}]$ can be obtained from

$$p_i^{\mathrm{eff}}(\mathbf{x}^{(1)},\mathbf{x}^{(2)}) = \left.\frac{\partial t^{\mathrm{eff}}(\mathbf{x},\mathbf{x}^{(2)})}{\partial x_i}\right|_{\mathbf{x}=\mathbf{x}^{(1)}}, \quad (i=1,2) \quad (3)$$

and

$$p_i^{\mathrm{ovr}}(\mathbf{x}^{(1)},\mathbf{x}^{(3)}) = \left.\frac{\partial t^{\mathrm{ovr}}(\mathbf{x},\mathbf{x}^{(3)})}{\partial x_i}\right|_{\mathbf{x}=\mathbf{x}^{(1)}}, \quad (i=1,2). \quad (4)$$

By equalizing time slopes, we find the location $\mathbf{x}^{(3)}$, for which the horizontal slownesses of the two events are identical,

$$p_i^{\mathrm{eff}}(\mathbf{x}^{(1)},\mathbf{x}^{(2)}) = p_i^{\mathrm{ovr}}(\mathbf{x}^{(1)},\mathbf{x}^{(3)}). \quad (5)$$

Therefore, the reflections $\mathbf{x}^{(1)}\mathbf{TQR}\mathbf{x}^{(2)}$ and $\mathbf{x}^{(1)}\mathbf{T}\mathbf{x}^{(3)}$ share the same downgoing leg $\mathbf{x}^{(1)}\mathbf{T}$. Similarly, equalizing the time slopes at point $\mathbf{x}^{(2)}$ helps to find the overburden reflection $\mathbf{x}^{(2)}\mathbf{R}\mathbf{x}^{(4)}$ that shares the upgoing leg $\mathbf{R}\mathbf{x}^{(2)}$ with the target event $\mathbf{x}^{(1)}\mathbf{TQR}\mathbf{x}^{(2)}$. The interval reflection traveltime can then be obtained from equation 1 discussed above. Since **T** and **R** represent the midpoints of the corresponding source-receiver pairs, their horizontal coordinates can be easily found from the coordinates of points $\mathbf{x}^{(1)}$, $\mathbf{x}^{(2)}$, $\mathbf{x}^{(3)}$, and $\mathbf{x}^{(4)}$.

Thus, the velocity-independent layer-stripping algorithm makes it possible to construct the interval moveout functions both in 2D and 3D, which can then be used for interval parameter estimation.

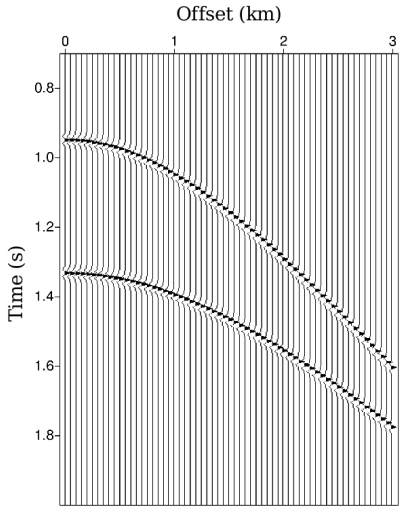

(a)

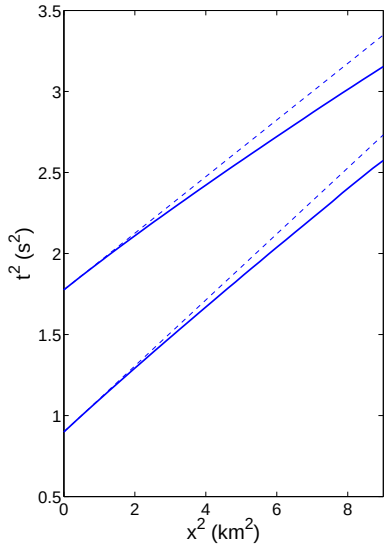

(b)

Figure 3. (a) Synthetic long-spread reflections from the top and bottom of layer 3 (target) in model 1. (b) The $t^2(x^2)$ function (solid lines) for both events in plot (a). The dashed lines mark the hyperbolic moveout function, $t^2 = t_0^2 + \frac{x^2}{V_{\rm nmo}^2}$. The model parameters are listed in Table 1.

3 TESTS ON SYNTHETIC DATA

Here, we test our layer-stripping algorithm on 2D and 3D long-spread P-wave data for layered VTI and orthorhombic models generated by anisotropic ray tracing (Gajewski & Pšenčík, 1987). The interval moveout parameters in the target layer are estimated from both our method and Dix-type equations. To evaluate the stability of the two techniques, we add several types of correlated noise to the input traveltimes.

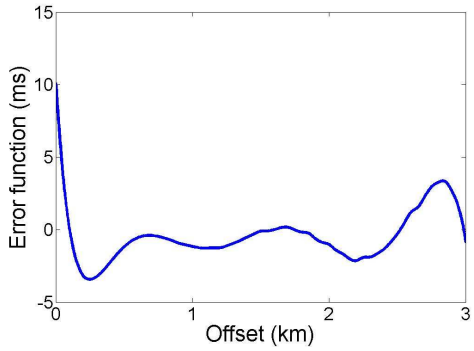

Figure 4. Random traveltime error with the maximum magnitude about 10 ms.

	Layer 1	Layer 2	Layer 3 (target)
Thickness (km)	0.7	0.3	0.5
t_0 (s)	0.70	0.25	0.39
$V_{\rm nmo}$ (km/s)	2.10	2.52	2.78
η	0	0.10	0.20

Table 1. Interval parameters of a three-layer VTI model (model 1)

.

3.1 2D inversion for VTI media

Nonhyperbolic moveout of P-waves in a single VTI layer can be accurately described by the following equation (Alkhalifah & Tsvankin, 1995; Tsvankin, 2005):

$$t^2 = t_0^2 + \frac{x^2}{V_{\rm nmo}^2} - \frac{2\eta\, x^4}{V_{\rm nmo}^2[\, t_0^2 V_{\rm nmo}^2 + (1+2\eta)x^2]}\,, \qquad (6)$$

where x is the offset, t_0 is the two-way zero-offset reflection traveltime, $V_{\rm nmo}$ is the normal-moveout velocity and η is the anellipticity coefficient. For layer-cake VTI media, all moveout parameters become effective quantities (Alkhalifah & Tsvankin, 1995; Tsvankin, 2005):

$$t^2(N) = t_0^2(N) + \frac{x^2}{V_{\rm nmo}^2(N)} - \frac{2\eta(N)\, x^4}{V_{\rm nmo}^2(N)\{t_0^2(N) V_{\rm nmo}^2(N) + [1+2\eta(N)]x^2\}}\,. \qquad (7)$$

The effective NMO velocity is obtained from the Dix equation,

$$V_{\rm nmo}^2(N) = \frac{1}{t_0(N)} \sum_{i=1}^{N} (V_{\rm nmo}^{(i)})^2\, t_0^{(i)}\,, \qquad (8)$$

where $t_0^{(i)}$ and $V_{\rm nmo}^{(i)}$ are the inte val values. The effective parameter η is approximately given by

$$\eta(N) = \frac{1}{8}\left\{ \frac{1}{V_{\rm nmo}^4(N) t_0(N)} \left[\sum_{i=1}^{N} (V_{\rm nmo}^{(i)})^4 (1 + 8\eta^{(i)})\, t_0^{(i)} \right] - 1 \right\}. \quad (9)$$

a: Command not found.

The best-fit effective parameters $V_{\rm nmo}$ and η for the top and bottom of a layer of interest are obtained by applying semblance-based nonhyperbolic moveout inversion to long-spread P-wave data. Then the interval $V_{\rm nmo}$ in layer i can be obtained from the Dix equation 8,

$$(V_{\rm nmo}^{(i)})^2 = \frac{V_{\rm nmo}^2(i)\, t_0(i) - V_{\rm nmo}^2(i-1)\, t_0(i-1)}{t_0(i) - t_0(i-1)}, \quad (10)$$

and the interval η can be found from equation 9:

$$\eta^{(i)} = \frac{1}{8(V_{\rm nmo}^{(i)})^4} \left[\frac{g(i) t_0^{(i)} - g(i-1) t_0^{(i-1)}}{t_0^{(i)} - t_0^{(i-1)}} - (V_{\rm nmo}^{(i)})^4 \right]; \quad (11)$$

$g(N) = V_{\rm nmo}^4(N)[1 + 8\eta(N)]$.

Although equations 6 and 7 provide a good approximation for nonhyperbolic moveout in VTI media, the estimated η is sensitive to small errors in $V_{\rm nmo}$ even if the maximum offset-to-depth ratio ($x_{\max}/h$) is between two and three. The tradeoff between the effective $V_{\rm nmo}$ and η (along with the slight bias of the nonhyperbolic moveout equation) causes the instability in the η estimation, which is amplified in the Dix-type layer stripping (Grechka & Tsvankin, 1998).

3.1.1 Model 1

The first numerical test was performed for the three-layer VTI model with the parameters listed in Table 1. We applied the velocity-independent layer stripping (VILS) and the Dix-type method to the synthetic long-spread ($x_{\max}/h = 2$ for the bottom of the model) data from the top and bottom of the target (third) layer (Figure 3). Note that, in Figure 3, the $t^2(x^2)$ curves for both events deviate obviously from the hyperbolic moveout approximation at large offsets. The absolute error of the interval η estimated by the VILS is 0.02, while it reaches 0.06 when the Dix-type method is used. The error of the VILS is mostly caused by the small bias of the single-layer moveout equation 6.

3.1.2 Error analysis

To study the influence of realistic noise on the interval parameter estimation, we added random, linear and sinusoidal time error to the reflection moveout from the bottom of the target layer. The traveltimes from the top of the target were left unchanged.

First, we used random errors with the magnitude of up to 10 ms (Figure 4). The errors in the interval η estimated by VILS do not exceed 0.02, while the Dix-type method produces errors in the range of 0.05–0.08. Since both methods are based on semblance analysis, they remain stable in the presence of random noise.

The second type of noise used in our tests is linear, which can simulate long-period static errors. For a relatively large error that changes from 6 ms at zero offset to -6 ms at the maximum offset, VILS estimates the interval $V_{\rm nmo}$ and η with errors of 4% and 0.07, respectively. The distortions in $V_{\rm nmo}$ and η after the Dix-type layer stripping are much larger (15% and 0.34, respectively), which makes the inversion results practically useless.

Next, we added the sinusoidal time errors, which can represent short-period static errors: $t = A\sin(n\pi x/x_{\max})$. The errors in the interval $V_{\rm nmo}$ and η estimated by both methods for different values of A and n are listed in Table 2. The error in the interval η produced by VILS reaches only 0.08 even for $A = 8$ ms, while the Dix-type method breaks down for $A > 3$ ms.

3.2 3D inversion for orthorhombic media

The azimuthally-dependent P-wave reflection moveout in a single orthorhombic layer can be well-approximated with azimuthally varying parameters $V_{\rm nmo}$ and η in equation 6 (Xu & Tsvankin, 2006; Vasconcelos & Tsvankin, 2006):

$$t^2(x,\alpha) = t_0^2 + \frac{x^2}{V_{\rm nmo}^2(\alpha)} - \frac{2\eta(\alpha)\, x^4}{V_{\rm nmo}^2(\alpha)[\, t_0^2\, V_{\rm nmo}^2(\alpha) + (1 + 2\eta(\alpha))x^2]}, \quad (12)$$

where α is the source-to-receiver azimuth. The azimuthally-dependent $V_{\rm nmo}$ is obtained from the equation of the NMO ellipse:

$$V_{\rm nmo}^{-2}(\alpha) = \frac{\sin^2(\alpha - \varphi)}{\left[V_{\rm nmo}^{(1)}\right]^2} + \frac{\cos^2(\alpha - \varphi)}{\left[V_{\rm nmo}^{(2)}\right]^2}, \quad (13)$$

where φ is the azimuth of the $[x_1, x_3]$ symmetry plane, and $V_{\rm nmo}^{(1)}$ and $V_{\rm nmo}^{(2)}$ are the NMO velocities in the vertical symmetry planes $[x_2, x_3]$ and $[x_1, x_3]$, respectively. The parameter η is approximately given by Pech & Tsvankin (2004):

$$\eta(\alpha) = \eta^{(1)} \sin^2(\alpha - \varphi) + \eta^{(2)} \cos^2(\alpha - \varphi) - \eta^{(3)} \sin^2(\alpha - \varphi)\cos^2(\alpha - \varphi), \quad (14)$$

where $\eta^{(1)}$, $\eta^{(2)}$, and $\eta^{(3)}$ are the anellipticity coefficients defined in the $[x_2, x_3]$, $[x_1, x_3]$, and $[x_1, x_2]$ symmetry planes, respectively.

For layered orthorhombic media, all moveout parameters become effective quantities. The effective

Error parameters	$A = 3$ ms, $n = 3$		$A = 3$ ms, $n = 2$		$A = 8$ ms, $n = 3$	
Inversion error	$V_{\rm nmo}$ (%)	η	$V_{\rm nmo}$ (%)	η	$V_{\rm nmo}$ (%)	η
VILS	0.6	0.01	0.0	0.00	2.1	0.08
Dix	11	0.19	8.2	0.13	21	0.41

Table 2. Percentage errors of the interval $V_{\rm nmo}$ and absolute errors of the interval η estimated by the velocity-independent layer stripping (VILS) and the Dix-type method (Dix) in the presence of a sinusoidal time error for model 1.

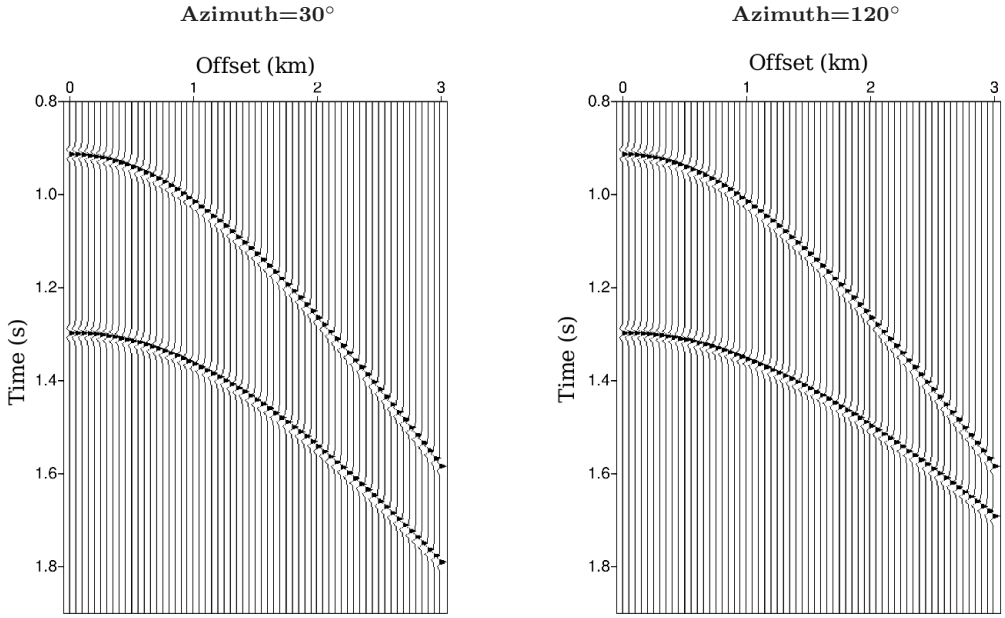

Figure 5. Synthetic long-spread reflections from the top and bottom of layer 3 (target) in model 2 (Table 3). The seismograms are computed in the two orthogonal vertical symmetry planes of the target orthorhombic layer.

$V_{\rm nmo}^{(1)}$, $V_{\rm nmo}^{(2)}$ and φ can be obtained from the generalized Dix equation for averaging of the interval NMO ellipses (Grechka *et al.*, 1999). If the vertical symmetry planes in different layers are misaligned, the principal directions for the effective η are described by a separate azimuth, φ_1 (Xu & Tsvankin, 2006):

$$\eta(\alpha) = \eta^{(1)} \sin^2(\alpha - \varphi_1) + \eta^{(2)} \cos^2(\alpha - \varphi_1) - \eta^{(3)} \cos^2(\alpha - \varphi_1) \sin^2(\alpha - \varphi_1)\,. \qquad (15)$$

The effective η value for each azimuth can be computed from equation 9, since kinematic signatures in each vertical plane of layered orthorhombic media can be approximately described by the corresponding VTI equation (Tsvankin, 1997, ,2005). Then the effective $\eta^{(1)}$, $\eta^{(2)}$, $\eta^{(3)}$ and φ_1 are found by fitting the effective η values to equation 15.

We use the semblance-based 3D nonhyperbolic moveout inversion algorithm of Vasconcelos & Tsvankin (2006) to estimate the best-fit effective moveout parameters $V_{\rm nmo}^{(1,2)}$, $\eta^{(1,2,3)}$, φ and φ_1 for the top and bottom of the target layer. Then the interval NMO ellipse is obtained from the generalized Dix equation (Grechka *et al.*, 1999), and the interval η value for each azimuth is computed from the VTI equation 11. Finally, the interval parameters $\eta^{(1,2,3)}$ are obtained by fitting the azimuthally varying η values to equation 14.

To apply VILS to 3D wide-azimuth data, we have to estimate both horizontal slowness components. In principle, the two orthogonal horizontal components of the slowness vector (equations 3 and 4) can be computed directly from reflection traveltimes on common-shot or common-receiver gathers. A more numerically stable option, however, is to use equation 12 with the b est-fit parameters to estimate the horizontal slownesses at each surface location. Despite the tradeoffs between the effective moveout parameters, equation 12 provides sufficient accuracy for long-spread P-wave moveout and, therefore, for the horizontal slowness components.

Error parameters	$A = 3$ ms, $n = 3$, $m = 0$		$A = 3$ ms, $n = 3$, $m = 2$		$A = 10$ ms, $n = 3$, $m = 0$	
Inversion error	$V_{\rm nmo}$ (%)	η	$V_{\rm nmo}$ (%)	η	$V_{\rm nmo}$ (%)	η
VILS	1.2	0.04	1.0	0.02	2.4	0.09
Dix	4.4	0.09	2.3	0.08	10	0.22

Table 3. Percentage maximum errors of the interval $V_{\rm nmo}^{(1,2)}$ and the absolute maximum errors of the interval $\eta^{(1,2,3)}$ in the presence of a sinusoidal time error in model 2. The errors in the estimated azimuth φ do not exceed 0.5° for both methods.

	Layer 1	Layer 2	Layer 3 (target)
Symmetry type	ISO	VTI	Orthorhombic
Thickness (km)	0.5	0.5	0.5
t_0 (s)	0.50	0.41	0.39
$V_{\rm nmo}^{(1)}$ (km/s)	2	2.49	3.18
$V_{\rm nmo}^{(2)}$ (km/s)	2	2.49	2.64
$\eta^{(1)}$	0	0.05	0.2
$\eta^{(2)}$	0	0.05	0.06
$\eta^{(3)}$	0	0	0.13
φ (°)			30

Table 4. Interval parameters of a three-layer model that includes an orthorhombic layer (model 2).

3.2.1 Model 2

The second model includes a target orthorhombic layer beneath the overburden composed of isotropic and VTI layers (Table 3). We applied both layer-stripping methods to the synthetic long-spread ($x_{\rm max}/h = 2$ for the bottom of the model), wide-azimuth data from the top and bottom of the target layer (Figure 5). Note that the traveltimes from the bottom of the target layer in Figure 5 vary with azimuth. Without traveltime noise, both methods give similar accuracy in the interval moveout parameters.

3.2.2 Error analysis

As before, we added linear and sinusoidal time error to the reflection moveout from the bottom of the target layer in model 2. For the linear error that changes from 6 ms at zero offset to -6 ms at the maximum offset for each azimuth, the interval $V_{\rm nmo}^{(1,2)}$ and $\eta^{(1,2,3)}$ estimated by VILS are distorted by no more than 3% and 0.06, respectively. In contrast, the Dix-type method produces the maximum errors of 9% and 0.16 in the interval $V_{\rm nmo}^{(1,2)}$ and $\eta^{(1,2,3)}$, respectively. The errors in the azimuth φ for both methods are negligible.

We also contaminated the traveltimes with several sinusoidal functions of the form $A\sin(n\pi x/x_{\rm max})\sin m\alpha$. The coefficients n and m control the period of the error function in the radial and azimuthal directions, respectively. When $m = 0$ (i.e., no azimuthal variation in the error), both methods get more accurate results when n is an even number (Table 4), which agrees with the conclusions of Xu & Tsvankin (2006). If the noise varies with azimuth, the errors in the inversion results are higher for the even values of m. VILS produces the errors not exceeding 0.09 in the interval η even for $A = 10$ ms, while Dix-type method gives unacceptably large errors of up to 0.22.

Thickness (km)	0.35		0.15	
Inversion error	$V_{\rm nmo}$ (%)	η	$V_{\rm nmo}$ (%)	η
VILS	2.2	0.05	8.3	0.15
Dix	7.5	0.13	20	0.38

Table 5. Errors of the interval $V_{\rm nmo}^{(1,2)}$ and $\eta^{(1,2,3)}$ for different thicknesses of the target layer in model 2 (Table 3) in the presence of the sinusoidal noise with $A = 3$ ms, $n = 3$ and $m = 0$.

Next, we studied the influence of the thickness of the target layer on the inversion results. Any layer-stripping method becomes less accurate as the layer gets thinner. We added the sinusoidal error with $A = 3$ ms, $n = 3$ and $m = 0$ to the traveltimes from the bottom of the target layer in model 2 and reduced the layer thickness from 0.5 km to 0.15 km (Table 5). Under this noise, VILS gives accurate values of both $V_{\rm nmo}$ and η even when the thickness is 0.2 km, while the error in the interval $V_{\rm nmo}$ estimated by the Dix-type method exceeds 8%. When the thickness decreases to 0.15km, even the errors from VILS become unacceptably large.

3.2.3 Model 3

The third model includes the target orthorhombic layer beneath the overburden composed of isotropic and orthorhombic layers (Table 6). Note that the vertical symmetry planes in the orthorhombic layers are misaligned, so the parameter η is described by equation 15. As was the case for model 2, the accuracy of both methods for noise-free data is similar.

The sinusoidal error $t = A\sin(n\pi x/x_{\rm max})$ applied to the traveltimes from the bottom of the target layer

	Layer 1	Layer 2	Layer 3 (target)
Symmetry type	ISO	ORTH	ORTH
Thickness (km)	0.3	0.7	0.5
t_0 (s)	0.30	0.58	0.39
$V_{\rm nmo}^{(1)}$ (km/s)	2	2.56	3.68
$V_{\rm nmo}^{(2)}$ (km/s)	2	3.06	2.73
$\eta^{(1)}$	0	0.05	0.24
$\eta^{(2)}$	0	0.07	0.12
$\eta^{(3)}$	0	0.02	-0.10
$\varphi\,(^\circ)$		30	70

Table 6. Interval parameters of a three-layer model that includes two orthorhombic layers with misaligned vertical symmetry planes (model 3).

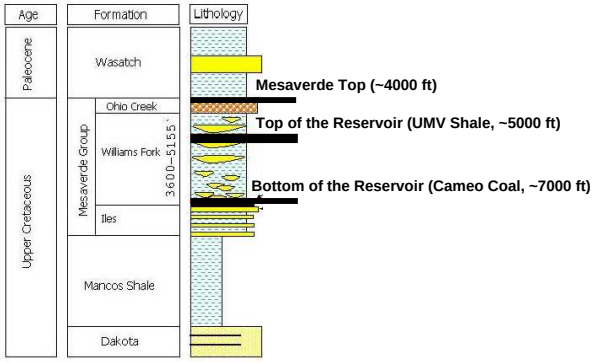

Figure 6. Stratigraphic column of Rulison field (after Xu & Tsvankin, 2007). The gas-producing reservoir is bounded by the UMV shale (the target layer in this study) and the Cameo coal.

produces much more significant distortions in the output of the Dix-type method compared to VILS. For instance, when $A = 6$ ms and $n = 3$, the maximum errors in the interval $V_{\rm nmo}$ and $\eta^{(1,2,3)}$ estimated by VILS are 4% and 0.09, respectively, while the Dix-type method produces the errors of 13% and 0.25, respectively.

4 FIELD-DATA EXAMPLE

We applied our 3D VILS algorithm to wide-azimuth P-wave data acquired at Rulison field, a basin-centered gas accumulation located in South Piceance Basin, Colorado. The reservoir (Williams Fork formation) is capped by the UMV shale, which served as the target layer in our study (Figure 6).

Xu & Tsvankin (2007) applied a comprehensive processing sequence designed for layered azimuthally

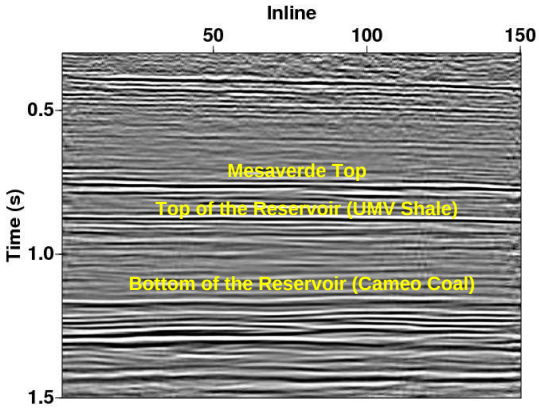

Figure 7. Seismic section across the middle of the survey area (after Xu & Tsvankin, 2007).

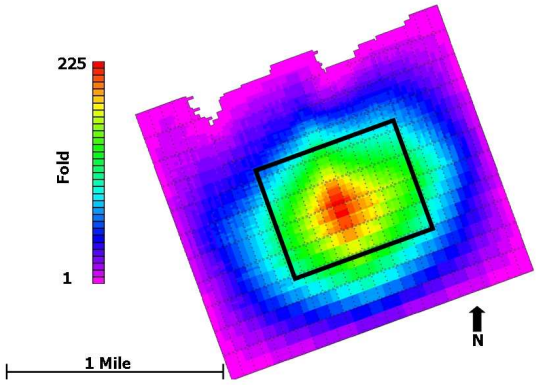

Figure 8. P-wave fold for the 55x55 ft bin size (after Xu & Tsvankin, 2007). The rectangle in the center marks the study area of our paper.

anisotropic media to the data and analyzed the azimuthal AVO response and the effective and interval NMO ellipses. We used the same data set as Xu & Tsvankin (2007), which was preprocessed for purposes of azimuthal moveout and AVO analysis. Since the subsurface structure is close to layer-cake (Figure 7), the moveout equations discussed above should give an accurate description of reflection traveltimes. To increase azimuth and offset coverage, we combined CMP gathers into 5x5 superbins, as suggested by Xu & Tsvankin (2007). We carried out the moveout inversion in the center of the RCP survey area (Figure 8), where the azimuthal coverage is sufficient for eliminating the acquisition footprint (Xu & Tsvankin, 2007).

Because the average offset-to-depth ratio at the bottom of the reservoir is close to unity, nonhyperbolic moveout inversion cannot be applied to the reservoir formation. Therefore, the target layer is chosen to be the UMV shale (cap rock), which overlies the reservoir. In the center of the study area, the offset-to-depth ratio at the bottom of the shale is between 1.9 and 2.2.

Superbin	1			2		
	$\eta^{(1)}$	$\eta^{(2)}$	$\eta^{(3)}$	$\eta^{(1)}$	$\eta^{(2)}$	$\eta^{(3)}$
VILS	0.38	0.47	-0.18	0.24	0.31	-0.15
Dix	0.74	1.24	-0.35	0.31	0.62	-0.19

Table 7. Interval parameters $\eta^{(1,2,3)}$ estimated for two superbin gathers in the center of the study area.

To estimate the interval moveout parameters, we used the VILS and Dix-type algorithms for the layered orthorhombic model discussed above.

Our tests show that the NMO ellipticity is small for both the top and bottom of the target layer over most of the area. Therefore, the principal directions of the effective and interval NMO ellipses are poorly constrained by the data. However, as long as the offset-to-depth ratio is close to two, the interval $\eta^{(1,2,3)}$ can be estimated in a reliable fashion. The interval parameters $\eta^{(1,2,3)}$ for two superbin gathers near the center of the area are listed in Table 7. The interval η values obtained by the Dix-type method are implausibly large for shale formations (Wang, 2002; Tsvankin, 2005).

To test the inversion stability of both methods, we also added a linear time error (from 4 ms at zero offset to -4 ms at the maximum offset for each azimuth) to the reflection moveout from the bottom of the shale layer in the second superbin. The interval $\eta^{(1,2,3)}$ estimated by VILS change only by -0.06, -0.07, 0.01, respectively, and the changes produced by the Dix-type method are much larger: -0.12, -0.21, 0.13, respectively. Hence, VILS is much more stable than the Dix-type method in the presence of correlated time errors, as was established above for the synthetic data.

The NMO ellipticity is pronounced only near the east boundary of the study area (Xu & Tsvankin, 2007). Due to the small offset-to-depth ratio (between 1 and 1.3) for the bottom of the target layer near the edges of the area, the effective parameters $\eta^{(1,2,3)}$ may contain large errors. The estimated interval $V_{\rm nmo}^{(1,2)}$ and φ for two adjacent superbin gathers near the east boundary are listed in Table 8. As before, we added a linear time error (from 2 ms at zero offset to -2 ms at the maximum offset for each azimuth) to the traveltimes from the bottom of the shale in the second superbin, which causes the deviation of 3% in the effective $V_{\rm nmo}^{(1,2)}$. As a result, the interval $V_{\rm nmo}^{(1,2)}$ and φ estimated by VILS change by 7%, 8% and 1°, respectively. In contrast, the changes from the Dix-type method are 13%, 16% and 4°, respectively. Due to the thin layer and relatively low semblance values (about 0.4) in 3D moveout analysis, the noise causes some significant deviations even in VILS. However, it is still beneficial to apply VILS for interval NMO velocity estimation from conventional-spread data.

5 DISCUSSION AND CONCLUSIONS

We applied the velocity-independent layer-stripping method (VILS) of Dewangan & Tsvankin (2006) to nonhyperbolic moveout inversion for layered VTI and orthorhombic media. While Dix-type differentiation algorithms operate with effective moveout parameters, VILS is based on stripping of reflection traveltimes. If the overburden is laterally homogeneous and has a horizontal symmetry plane, VILS produces the exact interval traveltime without any information about the velocity field. Then the interval traveltime function is inverted for the relevant parameters of the target layer using moveout equations for a homogeneous medium.

Because effective traveltimes are much better constrained by reflection data than effective moveout parameters, VILS gives more stable interval parameter estimates than Dix-type techniques. In particular, our synthetic tests on noise-contaminated data confirm that VILS can substantially increase the accuracy of nonhyperbolic moveout inversion for the interval time-processing parameter η in VTI media. The addition of small linear or sinusoidal time errors causes pronounced distortions in the effective η values, which get further enhanced by Dix-type layer stripping. In contrast, the interval moveout function produced by VILS is weakly sensitive to moderate levels of noise in the input traveltimes, which ensures a higher stability of the interval η estimates.

We also discussed the extension of VILS to 3D wide-azimuth P-wave data from azimuthally anisotropic models that include orthorhombic and TI layers. To identify the target and overburden reflections that share the same ray segments, we compute the horizontal slowness components from the best-fit effective moveout parameters, which helps to avoid direct differentiation of traveltimes and to reduce the computational cost. Then the interval moveout produced by VILS is inverted for the azimuths of the vertical symmetry planes, symmetry-direction NMO velocities, and the anellipticity parameters $\eta^{(1,2,3)}$. Wide azimuthal coverage helps to increase the stability of η estimation using 3D Dix-type layer stripping. Still, our tests clearly demonstrate the superior per formance of VILS for typical orthorhombic models, inlcuding those with the depth-varying azimuths of the symmetry planes.

The 3D version of the method was successfully tested on wide-azimuth P-wave reflections from an anisotropic shale layer at Rulison field in Colorado. For long-spread superbin gathers in the center of the study area, VILS yields more plausible and stable values of the interval parameters $\eta^{(1,2,3)}$ than the Dix-type method. Near the east boundary of the study area, where the offset-to-depth ratio is smaller and the η-parameters are poorly constrained, application of VILS helps to obtain a more stable estimate of the interval NMO ellipse.

While our results clearly demonstrate the advantages of our method over Dix-type techniques, the su-

Superbin	1			2		
	$V_{\rm nmo}^{(1)}$ (km/s)	$V_{\rm nmo}^{(2)}$ (km/s)	φ (°)	$V_{\rm nmo}^{(1)}$ (km/s)	$V_{\rm nmo}^{(2)}$ (km/s)	φ (°)
VILS	4.22	3.99	115	4.33	3.84	122
Dix	4.26	3.82	104	4.41	3.91	139

Table 8. Interval NMO ellipses estimated for two superbin gathers near the east boundary of the study area.

perior accuracy of VILS is achieved at the expense of relatively high computational cost. In addition to estimating and matching reflection time slopes at the surface, it is necessary to carry out nonhyperbolic moveout inversion not only for recorded reflection events, but also for the interval moveout function.

Similar to the original version of the PP+PS=SS method, our layer-stripping algorithm operates with reflection traveltimes. Grechka & Dewangan (2003) developed an efficient implementation of the PP+PS=SS method by replacing traveltime analysis with a convolution of recorded PP and PS traces. Their algorithm can be adapted to compute interval P-wave reflection data using the reflections from the top and bottom of the target layer. Although the convolution of recorded traces cannot produce the correct amplitudes, the constructed data have the kinematics of P-wave primary reflections and, therefore, are suitable for interval moveout analysis.

6 ACKNOWLEDGMENTS

We are grateful to Pawan Dewangan (CWP, now NIO, India), Ivan Vasconcelos (CWP, now ION), Xiaoxia Xu (CWP, now ExxonMobil), Jyoti Behura (CWP/CSM) and Dirk Gajewski (UH, Germany) for making available their codes and numerous helpful suggestions. We would like to thank Tom Davis and Bob Benson (both of RCP/CSM) for providing the seismic data from Rulison field. We are also grateful to our CWP colleagues for valuable discussions and technical help. This work was supported by the Consortium Project on Seismic Inverse Methods for Complex Structures at CWP and by the Chemical Sciences, Geosciences and Biosciences Division, Office of Basic Energy Sciences, Office of Science, U.S. Department of Energy.

References

Alkhalifah, T. 1997. Velocity analysis using nonhyperbolic moveout in transversely isotropic media. *Geophysics*, **62**, 1839–1854.

Alkhalifah, T., & Tsvankin, I. 1995. Velocity analysis for transversely isotropic media. *Geophysics*, **60**, 1550–1566.

Bakulin, A., Grechka, V., & Tsvankin, I. 2000. Estimation of fracture parameters from reflection seismic data –Part II: Fractured models with orthorhombic symmetry. *Geophysics*, **65**, 1803–1817.

Dewangan, P., & Tsvankin, I. 2006. Velocity-independent layer stripping of PP and PS reflection traveltimes. *Geophysics*, **71**, U59–U65.

Dix, C. H. 1955. Seismic velocities from surface measurements. *Geophysics*, **20**, 68–86.

Gajewski, D., & Pšenčík, I. 1987. Computation of high frequency seismic wavefields in 3-D laterally inhomogeneous anisotropic media. *Geophysical Journal of the Royal Astronomical Society*, **91**, 383–412.

Grechka, V., & Dewangan, P. 2003. Generation and processing of pseudo-shear-wave data: Theory and case study. *Geophysics*, **68**, 1807–1816.

Grechka, V., & Kachanov, M. 2006. Seismic characterization of multiple fracture sets: Does orthotropy suffice? *Geophysics*, **71**, D93–D105.

Grechka, V., & Tsvankin, I. 1998. Feasibility of nonhyperbolic moveout inversion in transversely isotropic media. *Geophysics*, **63**, 957–969.

Grechka, V., & Tsvankin, I. 1999. 3-D moveout velocity analysis and parameter estimation for orthorhombic media. *Geophysics*, **64**, 820–837.

Grechka, V., & Tsvankin, I. 2002. PP+PS=SS. *Geophysics*, **67**, 1961–1971.

Grechka, V., Tsvankin, I., & Cohen, J.K. 1999. Generalized Dix equation and analytic treatment of normal-moveout velocity for anisotropic media. *Geophysical Prospecting*, **47**, 117–148.

Grechka, V., Tsvankin, I., & Cohen, J.K. 2002. Multicomponent stacking-velocity tomography for transversely isotropic media. *Geophysics*, **67**, 1564–1574.

Pech, A., & Tsvankin, I. 2004. Quartic moveout coefficient for a dipping azimuthally anisotropic layer. *Geophysics*, **69**, 699–707.

Schoenberg, M., & Helbig, K. 1997. Orthorhombic media: Modeling elastic wave behavior in a vertically fractured earth. *Geophysics*, **62**, 1954–1974.

Stork, C. 1992. Reflection tomography in the post migrated domain. *Geophysics*, **57**, 680–692.

Toldi, J., Alkhalifah, T., Berthet, P., Arnaud, J., Williamson, P., & Conche, B. 1999. Case study of estimation of anisotropy. *The Leading Edge*, **18**, 588–594.

Tsvankin, I. 1997. Anisotropic parameters and P-wave velocity for orthorhombic media. *Geophysics*,

62, 1292–1309.

Tsvankin, I. 2005. *Seismic signatures and analysis of reflection data in anisotropic media, 2nd edition*. Elsevier Science Publ. Co., Inc.

Vasconcelos, I., & Tsvankin, I. 2006. Nonhyperbolic moveout inversion of wide-azimuth P-wave data for orthorhombic media. *Geophysical Prospecting*, **54**, 535–552.

Wang, Z. 2002. Seismic anisotropy in sedimentary rocks, part 2: Laboratory data. *Geophysics*, **67**, 1423–1440.

Xu, X., & Tsvankin, I. 2006. Anisotropic geometrical-spreading correction for wide-azimuth P-wave reflections. *Geophysics*, **71**, D161–D170.

Xu, X., & Tsvankin, I. 2007. A case study of azimuthal AVO analysis with anisotropic spreading correction. *The Leading Edge*, **26**, 1552–1561.